QUARTERLY JOURNAL OF THE ROYAL METEOROLOGICAL SOCIETY
*Q. J. R. Meteorol. Soc.* (2009)
Published online in Wiley InterScience
(www.interscience.wiley.com) DOI: 10.1002/qj.451

# The diurnal cycle of surface divergence over the global oceans

R. Wood,[a]* M. Köhler,[b] R. Bennartz[c] and C. O'Dell[c]
[a]*University of Washington, Seattle, USA*
[b]*European Center for Medium-Range Weather Forecasts, Reading, UK*
[c]*University of Wisconsin, Madison, USA*

**ABSTRACT:** The diurnal cycle of surface divergence over the oceans is examined using 4 × daily data from the tandem SeaWinds satellite missions during April–September 2003. A statistically significant diurnal cycle of surface divergence is observed over a large fraction of the tropical and subtropical oceans. The highest amplitudes are found adjacent to tropical landmasses and decrease exponentially with distance away from the coast, with a representative *e*-folding distance of approximately 200 km. In most of these near-coastal regions the surface divergence peaks at ∼15–20 h locally and there is evidence of offshore propagation of the signal. There are regions, however, where strong cycles persist for much greater distances offshore. Over the southeast Pacific Ocean, there is evidence of a diurnal subsidence wave that propagates for over 2000 km away from the South American coast at approximately 25 m $s^{-1}$. A cloud response to the subsidence wave moving westward from the Andes mountains is detected using passive microwave observations of liquid-water path. Over the remote tropical Pacific, significant diurnal amplitude is found in and around regions of strong mean surface convergence, with a phase suggesting a surface response to the early morning diurnal maximum in precipitation and propagation away from these sources consistent with gravity waves forced by deep tropospheric heating. European Centre for Medium-Range Weather Forecasts (ECMWF) model simulations of 850 hPa subsidence show a diurnal cycle that is largely consistent with the SeaWinds divergence observations. Copyright © 2009 Royal Meteorological Society

KEY WORDS surface divergence; diurnal; scatterometer; subsidence wave

*Received 18 April 2008; Revised 30 April 2009; Accepted 1 May 2009*

## 1. Introduction

Large-scale vertical motion in the lower atmosphere is associated with mean convergence/divergence of the surface winds. These convergence/divergence patterns can be detected over the oceans using satellite scatterometer data (Zheng *et al*., 1997) and yield a wide variety of information on vertical atmospheric motions occurring over a wide array of time and space scales. These can be useful both for the purposes of being able to forecast weather systems better (Atlas *et al*., 2001; Isaksen and Janssen, 2004) and for understanding dynamical processes occurring in the atmosphere (Chelton *et al*., 2004) and ocean (Kessler, 2002).

Single-satellite scatterometery provides some information on the diurnal cycle of ocean surface winds, but sampling is generally limited to twice daily at best. The SeaWinds tandem scatterometer missions (Lungu, 2002), however, allowed four-times-daily sampling during a six-month period (April–September 2003) with the same instrument design (SeaWinds) on two satellites (QuikSCAT at ∼0600 and 1800 h local, and ADEOS-II at ∼1030 and 2230 h local).

*Correspondence to: R. Wood, Department of Atmospheric Sciences, Box 351640, University of Washington, Seattle, WA 98915, USA.
E-mail: robwood@atmos.washington.edu

Scatterometer data have been used previously to study the diurnal cycle of surface winds using QuikSCAT alone (Gille *et al*., 2003) and using the tandem mission (Gille *et al*., 2005). These analyses revealed rich patterns of diurnal wind variability, including wind reversals in near-coastal regions that are clear signs of land/sea-breeze circulations. The Gille *et al*. (2005) results also demonstrate a significant diurnal cycle of surface winds across most of the remote tropical Pacific and Atlantic Oceans. Using surface meteorological marine reports, Dai and Deser (1999) have suggested that the remote tropical ocean diurnal cycle is an equatorially symmetric response to the diurnal cycle of tropical convection, but this conclusion is uncertain due to sampling noise.

In this article we describe aspects of the diurnal cycle of surface divergence, rather than the wind components themselves, over the bulk of the global oceans using SeaWinds data complemented by vertical wind information from European Centre for Medium-Range Weather Forecasts (ECMWF) analysis fields.

## 2. Methods

We use SeaWinds scatterometer 10 m wind measurements collected during April–September 2003. Input wind data are from the Jet Propulsion Laboratory Physical Oceanography Data Archive (PO-DAAC) and are gridded on a

$0.25^\circ \times 0.25^\circ$ global grid. There is one grid for each of the ascending and descending passes from each of the QuikSCAT and ADEOS-II satellites. Data contaminated by rain are removed. These data are used to create, for each of the ascending and descending overpass grids for each satellite, mean wind-component maps at $0.25^\circ \times 0.25^\circ$ resolution for the six-month period extending from 60°S to 60°N. Divergence fields are derived from these maps using centred differencing at the four overpass times. Next, to reduce noise we aggregate these data on to a $2.5^\circ \times 2.5^\circ$ grid. The divergence diurnal cycle is analysed for each oceanic grid box using a Fourier decomposition after first linearly interpolating the data temporally for the four mean overpass times (which vary with latitude) on to equally spaced local times (0, 6, 12, 18 h). This decomposition yields the mean, amplitude and phase of the first diurnal harmonic. In this study we do not use the limited information about the semidiurnal cycle as it is poorly sampled with $4 \times$ daily sampling, and therefore inconclusive.

A 10 day forecast using the 40 km resolution ECMWF model was performed for each of the six months (April–September 2003). Data were produced eight times per day (0000, 0300, 0600 UTC, etc.) and then averaged in time and gridded using linear interpolation on to a $5^\circ \times 5^\circ$ grid to reduce sampling noise. The key variable, vertical velocity, was specially diagnosed consistent with semi-Lagrangian advection to avoid the conversion of omega to vertical velocity, which is complicated by the semi-diurnal tidal wave. Details are given in the Appendix. The model variable in this study is 850 hPa vertical wind field $w_{850}$, which is used in comparisons with the surface-convergence data from SeaWinds which are themselves regridded for the purpose on to a $5^\circ \times 5^\circ$ grid. Quikscat surface winds are assimilated into the ECMWF variational analysis. Chelton and Freilich (2005) compared the ECMWF analyzed surface winds (with QuikScat) assimilation) with scatterometer and buoy data. They documented a 0.4 m $s^{-1}$ wind-speed low bias and rms model/QuikScat differences of 1.0–2.5 m $s^{-1}$ with the lowest values in the trade-wind regions such as those off the Chilean/Peruvian coast. This rms difference includes an estimated QuikScat random error of 0.75 m $s^{-1}$ in the along-wind direction.

## 3. Results

### 3.1. Near-global maps

Figure 1 shows maps of the mean surface divergence $D_0$, the diurnal amplitude and the local time of maximum divergence from SeaWinds, and the corresponding data for the 850 hPa subsidence rate from ECMWF. The mean divergence and subsidence fields clearly delineate the major features of Boreal summer climatology, including the extensive regions of divergence and corresponding subsidence over the eastern subtropical oceans, strongly convergent intertropical convergence zones (ITCZs) in the eastern Pacific and Atlantic Oceans, the South Pacific Convergence Zone (SPCZ) and the broader regions of convergence and mean ascent in the tropical West Pacific and Indian Oceans. Regions of mean large-scale midlatitude convergence are also evident, as are smaller scale convergence/divergence features, especially in the Southern Ocean. These may be related to mesoscale sea-surface-temperature anomalies associated with oceanic fronts and eddies that are quasi-stationary or move relatively slowly (Xie, 2004; Chelton *et al*., 2004; Small *et al*., 2008) compared with the six months of observations used here.

The diurnal amplitude (Figure 1(b)) is largest close to coastlines, especially those in the tropics, exceeding $2 \times 10^{-6}$ $s^{-1}$ in many places, and comparable to the typical mean convergence rates. As with the mean fields, there is a good correspondence between strong divergence amplitude and strong 850 hPa subsidence amplitude in the ECMWF model, although there are some notable exceptions such as over the Atlantic Ocean. Especially over the region to the north-east of South America, the regions of poor correspondence in diurnal amplitude are also regions where the mean fields differ considerably.

The coastal diurnal cycle is far from uniform in amplitude. There are also extensive regions well away from coastlines with significant diurnal amplitude. For example, the region to the west of South America, extending over 2000 km offshore, has a large diurnal amplitude in both surface divergence and 850 hPa subsidence. In addition, significant amplitude exists in the narrow zones of strong convergence over the tropical Pacific, although this is more striking in the observations than in the EMCWF model fields. Few of the signals in midlatitudes are statistically significant in either the observations or the model. This does not necessarily preclude diurnal variability there, but reflects greater variability, which reduces the signal-to-noise ratio. However, we note that the reduced Rossby radius in the midlatitudes would also reduce the propagation distance for internal waves. A longer record than we currently have will be needed to determine whether there are significant diurnal cycles in the midlatitudes.

Many of the broad features in Figure 1(b) agree well with the analysis of ship and land-station reports carried out by Dai and Deser (1999), but the amplitudes we observe are considerably greater, by approximately a factor of two or so. The reason for this is unclear. Also, the improved sampling of the scatterometers compared with ships resolves some of the weaker but coherent features across the remote tropical Pacific and south-east Pacific that are not clearly evident in the analysis of *in situ* data.

In coastal regions the divergence and subsidence predominantly peaks in the afternoon and early evening (Figure 1(c) and (f)), a pattern consistent with the land/sea-breeze circulation (Rotunno, 1983), and supports the previous analysis from SeaWinds (Gille *et al*., 2005). We discuss this further in section 3.3. In section 3.4 we examine the interesting diurnal variability over the remote tropical Pacific.



DOI: 10.1002/qj

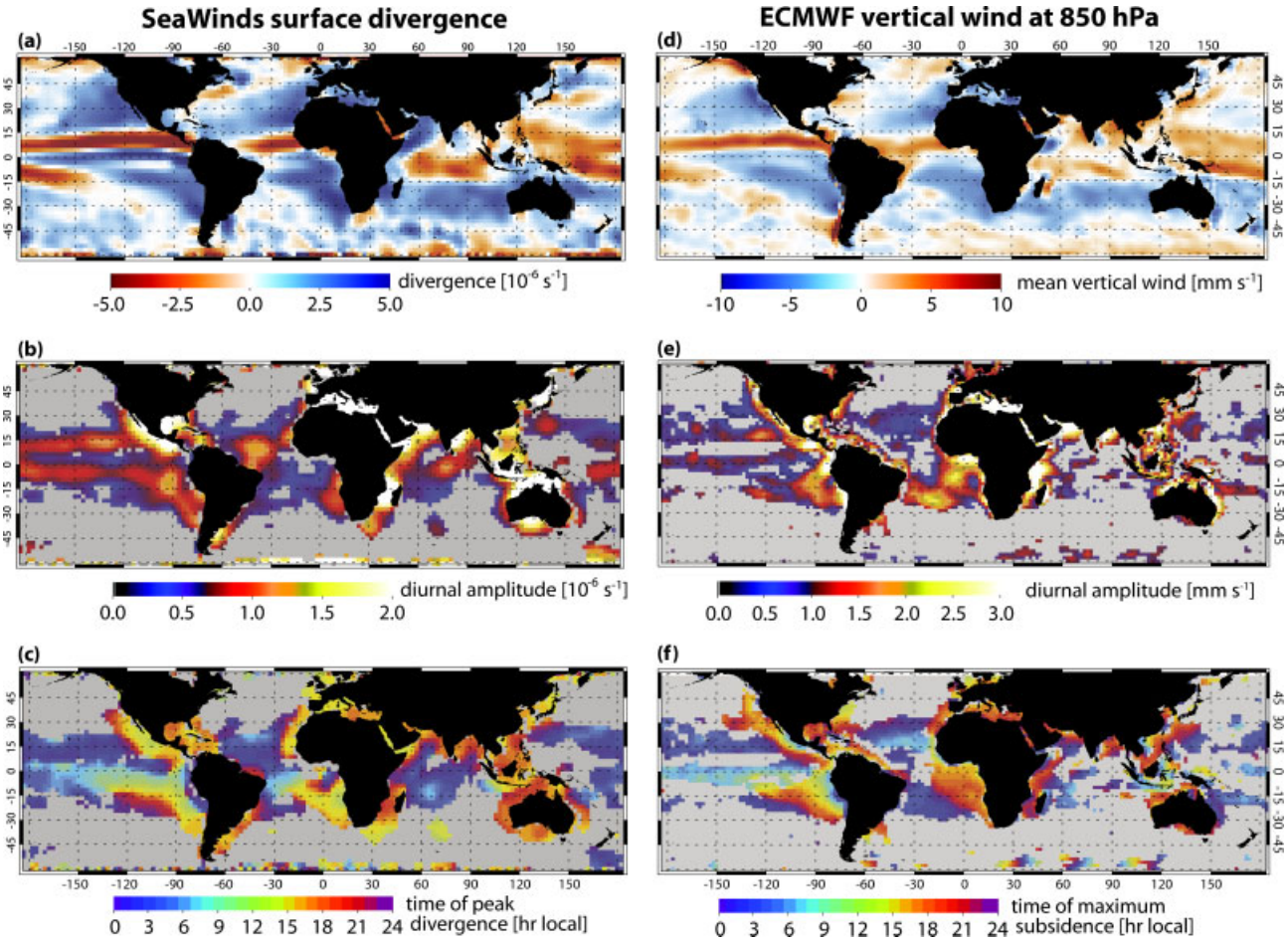


Figure 1. Mean (a), diurnal amplitude (b), and local time of maximum diurnal surface divergence (c) for April–September 2003 from the tandem SeaWinds data (left panels). Mean (d), diurnal amplitude (e), and local time of maximum diurnal subsidence at 850 hPa (f) from the ECMWF forecast data (right panels). Only regions for which the diurnal amplitude is statistically significantly different from zero at the 95% level are coloured. This figure is available in colour online at www.interscience.wiley.com/journal/qj

An unexpected and interesting feature of Figure 1(c) and (f) is the wave-like signals emanating from several stretches of the tropical coastlines that clearly propagate in time hundreds or even thousands of kilometres to the remote oceans. The most notable of these *subsidence waves* are seen over the southeast Pacific and to the west of Mexico and Central America. We examine these waves in more detail in section 3.5.

### 3.2. Divergence and vertical wind diurnal cycles

Figure 2 compares the time mean, diurnal amplitude and phase of the diurnal cycle of surface divergence (abscissae) with the respective time mean, diurnal amplitude and phase of the 850 hPa vertical wind field (ordinates) from the ECMWF analyses. The mean fields (Figure 2(a)) are closely connected, which is expected because the spatial variability of the time-mean surface divergence is a signature of the atmospheric general circulation that extends through the troposphere. Moreover the data suggest that the mean divergence is roughly constant with height from the surface to 850 hPa in regions where the mean vertical velocity is relatively weak, but decreases with height in regions of strong surface convergence (i.e. the ITCZ regions, especially in the eastern Pacific and Atlantic, see Figure 1). Assuming a quadratic vertical velocity profile, one can infer the level $z_{\max}$ at which the vertical velocity must peak, i.e.

$$z_{\max} = \frac{1}{2}\frac{z_{850}}{\left(1 - \dfrac{w_{850}}{D_0 z_{850}}\right)}, \tag{1}$$

where $z_{850}$ is the height of the 850 hPa level (approximately 1500 m). For strongly convergent regions (Figure 2), $w_{850}/D_0 z_{850} \sim 0.5$ suggesting that $z_{\max} \sim$ 1500 m. Interestingly, this is close to the height of maximum vertical velocity for strongly convergent regions of the eastern Pacific found in Back and Bretherton (2006).

While the diurnal amplitudes are significantly correlated ($r = 0.60$, Figure 2(b)), sampling noise is substantially greater than for the mean state. However, a comparison of the phase of the diurnal cycle (Figure 2(c)) reveals that the diurnal cycle of $w_{850}$ and that of surface divergence are in phase, suggesting that the diurnal signals in the scatterometer data are consistent with a



DOI: 10.1002/qj

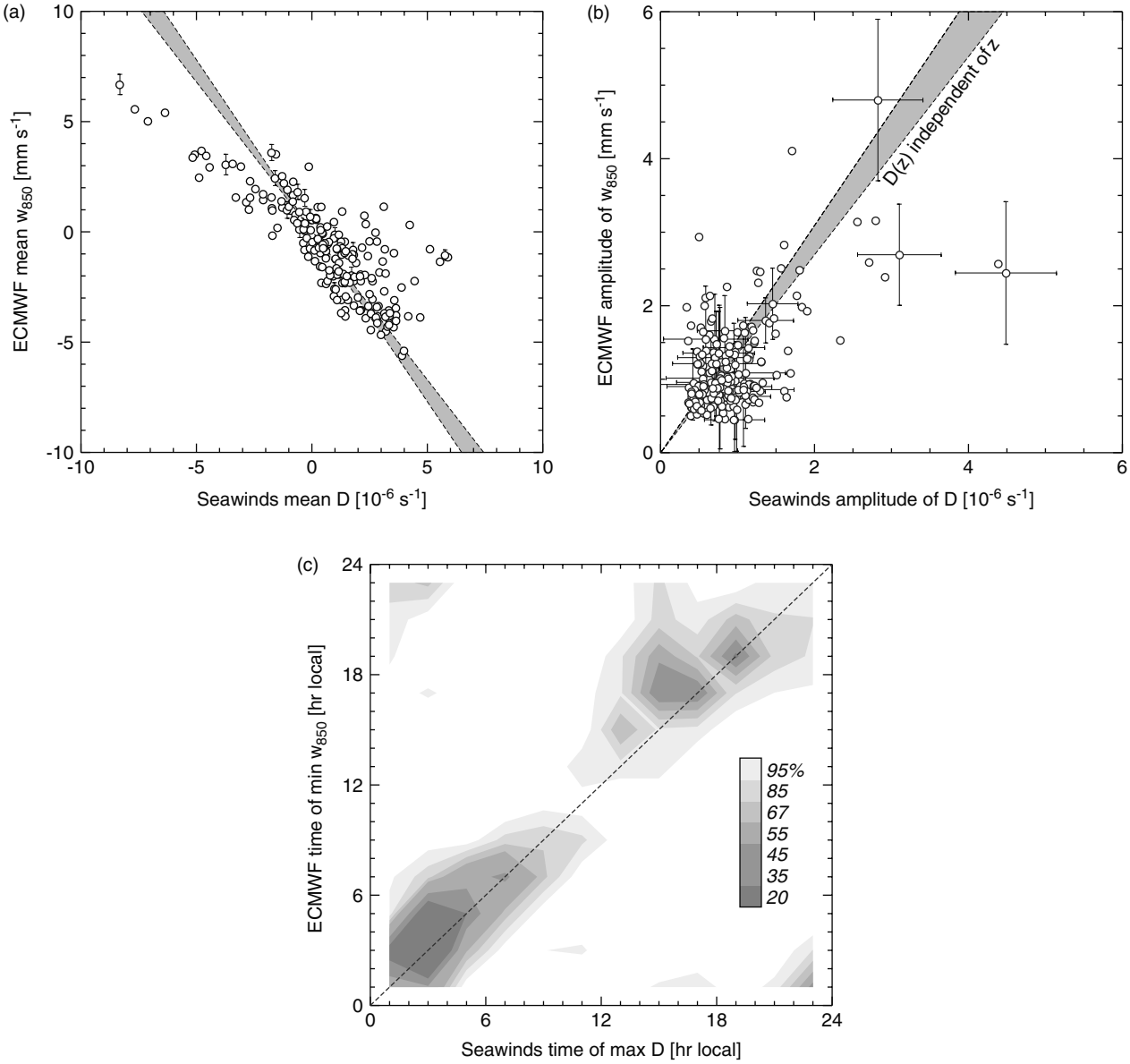


Figure 2. (a) Time-mean surface divergence $D_0$ from SeaWinds against mean vertical wind at 850 hPa $w_{850}$ from the ECMWF model. The data have been binned into $5^\circ \times 5^\circ$ regions over the ocean (60°S–60°N). (b) As for (a), but a comparison of the amplitude of the diurnal cycle rather than the mean, and only those regions with an amplitude that is determined to be statistically distinguishable from zero at the $1\sigma$ level are shown. The grey areas on (a) and (b) assume a constant divergence from the surface to 850 hPa, with the spread being that caused by variability in the height of the 850 hPa surface given seasonal and geographic variability in surface pressure and lower tropospheric temperature. Error bars represent sampling errors in the mean or the fitting error for diurnal amplitude, at the $1\sigma$ level. (c) Comparison of the phase of the diurnal cycle, i.e. a joint pdf of the SeaWinds time of maximum $D_0$ and ECMWF time of minimum $w_{850}$, where the darkness of the grey-scale indicates the density of points. The scale bar shows what fraction of the total joint pdf is contained in colours darker than the colour indicated.

mode of diurnal variability extending above the boundary layer. Indeed, the phases of $w_{850}$ and $D_0$ remain in good agreement at 700 hPa, but the agreement is much poorer at 500 hPa (not shown), suggesting that the processes responsible for the diurnal cycle in surface divergence are generally confined to the lowest half of the troposphere.

### 3.3. Near-coastal diurnal cycle

Figure 3 demonstrates that equatorward of 30°N and S the regions where the diurnal amplitude in $D_0$ is strongest are most frequently found to be within 4–5° of the coast, and that in these regions $D_0$ most typically peaks during the late afternoon (Figure 3(a)). This is consistent with the expected pattern for a sea-breeze circulation, and is behaviour consistent with Gille *et al.* (2005). The strength of the surface sea-breeze response decreases approximately exponentially with distance away from the coast, with an $e$-folding distance of approximately 200 km. This is consistent with the linear theory of the sea breeze as elucidated by Rotunno (1983), where for latitudes equatorward of 30° the horizontal influence of the sea-breeze circulation extends to a distance $L = NH(\omega^2 - f^2)^{-1/2}$, where $N$



DOI: 10.1002/qj

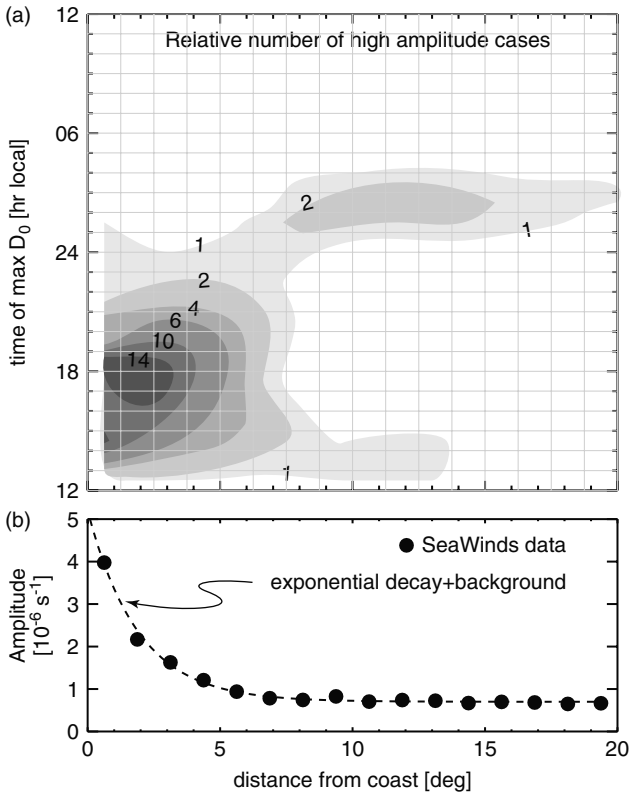


Figure 3. (a) The number of 2.5° × 2.5° regions in the tropics (30°S–30°N) that have a statistically significant and strong (amplitude greater than $10^{-6}$ $s^{-1}$) diurnal cycle of $D_0$ with a given phase (one-hour intervals) as a function of the distance from the nearest coastline. (b) The mean amplitude of the diurnal cycle for all locations with a statistically significant diurnal cycle in $D_0$ as a function of distance from the coast. The dashed line shows an exponential decay with an $e$-folding distance of 1.9°, and a far-field amplitude of $0.7 \times 10^{-6}$ $s^{-1}$.

is the Brunt–Väisälä frequency, $H$ is the depth of the heating, $\omega$ is the diurnal frequency and $f$ is the Coriolis parameter. For a 1 km deep heating, typical of the sea-breeze circulations within the boundary layer that form around relatively flat coastlines due to surface-heating contrasts, the value of $L$ increases from about 150 km at the Equator to about 300 km at 20°N and S. These values are consistent with the 200 km $e$-folding distance for the amplitude of the near-coastal observations in Figure 3(b), but breakdown of the observations by latitude did not reveal any significant latitudinal variations from 30°S to 30°N. It is unclear why this is.

Another interesting feature of the near-coastal diurnal cycle is that there is considerable geographical variability in the amplitude, with the strongest cycles being found in regions where the coastline is relatively convex on length-scales of up to a few times the $e$-folding distance (Figure 1(b) and (e)). For example, while regions such as the Gulf of Mexico, the Arabian Gulf and the area between Madagascar and mainland Africa have very strong amplitudes, other regions such as much of the eastern coast of South America, far eastern and western coasts of Australia and South Africa, with more concave coastlines, do not exhibit such strong diurnal variability. The constructive interference of multiple land–sea breezes is hypothesized to be responsible for such behaviour.

Other near-coastal regions in the tropics show remarkably weak diurnal variability in surface divergence. The Brazilian coastline and the Gulf of Guinea are two such areas (Figure 1(b)). It is curious that in both of these regions ECMWF shows significant diurnal amplitude in the vertical wind, inconsistent with the generally tight relationship between the diurnal cycle of surface divergence and wind discussed in Section 3.2. In both these regions, the prevailing flow is predominantly onshore during April to September, and observations suggest that this can impact the propagation speed and spatial structure of the sea-breeze circulation (Atkins and Wakimoto, 1997). A more detailed analysis of the impact of prevailing flow is beyond the scope of this study.

### 3.4. Tropical remote ocean

Figure 4 shows that over the remote tropical oceans, where the influence of land is minimal, regions with mean surface convergence tend to exhibit a strikingly different diurnal cycle from divergent regions. In most convergent regions $D_0$ tends to peak between 2 and 6 am local time. In divergent regions the time of peak divergence tends to be more evenly distributed throughout the day. Having said this, it may be notable that there is still a preference for $D_0$ to peak during the later night and early-morning hours in divergent regions, and at a delayed hour compared with convergent regions.

The data in Figure 1(c) are consistent with an analysis of surface divergence from tropical Pacific surface-wind measurements within 8° of the equator (Deser and Smith, 1998). Both show surface divergence peaking at approximately 0800 local time. The phase lines aligned east–west suggest that this reflects the time taken for the diurnal wave to propagate from its source, the ITCZ.

Whether this behaviour is consistent with the idea of diurnal strengthening and weakening of the Hadley cells, as suggested by the analysis of ship surface-wind reports in Dai and Deser (1999), is not clear. Insofar as the diurnal cycle of surface divergence can be interpreted in this way, a comparison of the diurnal amplitude with the mean convergence indicates that the oceanic Hadley cell may undergo a diurnal cycle with an amplitude of some 10–20% of the mean. From the scatterometer data (Figure 4) it is inferred that the Hadley cell would be weakest during the early-morning hours, which contrasts with the late-evening weakening suggested by the analysis of Dai and Deser (1999). However, the spatial smoothing used in Dai and Deser (1999) to reduce noise may have resulted in a loss of the intricate spatial variability that is revealed by the scatterometer data.

Precipitation, and therefore convective heating from oceanic tropical deep convection, peaks during the late-evening and early morning hours (Nesbitt and Zipser, 2003; Yang and Smith, 2006). The behaviour in Figure 4 appears consistent with the generation of diurnal gravity waves by deep convective heating; these then propagate



DOI: 10.1002/qj

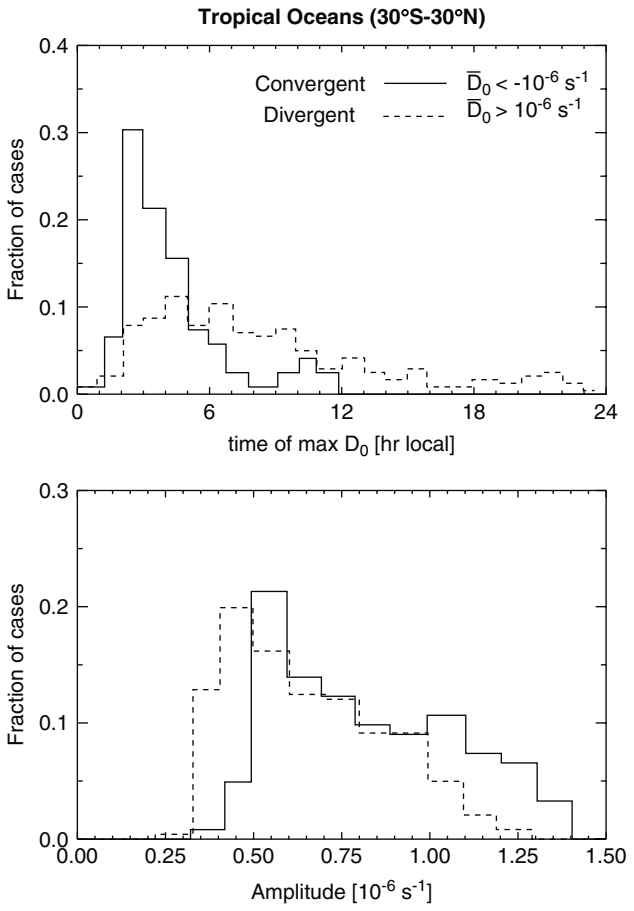


Figure 4. Histograms of (a) the time of maximum $D_0$ and (b) the diurnal $D_0$ amplitude for $2.5^\circ \times 2.5^\circ$ regions with statistically significant diurnal cycles over the remote ($>20^\circ$ from the nearest coast) tropical ($30^\circ$S–$30^\circ$N) oceans. Different histograms are shown for regions where the mean $D_0 > 10^{-6}$ s$^{-1}$ (divergent regions, dashed lines) and where $D_0 < -10^{-6}$ s$^{-1}$ (convergent regions, solid lines).

away from the heat sources to adjacent regions of mean subsidence.

A striking example of propagating internal gravity waves from deep convection can be seen by examination of the region to the south of the East Pacific ITCZ (110–130°W) in Figure 1. In the ITCZ region itself (7–16°N) the peak $D_0$ occurs during the early morning hours. The peak $D_0$ becomes progressively later as one moves south over the divergent regions, finally peaking during the late evening at 20°S, 110–120°W where on its eastern edge it merges with the southeast Pacific wave (see section 3.5.2 below). This propagation speed is $\sim$50 m s$^{-1}$, consistent with an internal wave (see section 3.5.2) caused by heating extending up to approximately 13 km. This is in excellent agreement with the depth of convective latent heating for tropical deep convection, which peaks at about 7–8 km and extends to 12–14 km (Shige *et al*., 2007).

## 3.5. Diurnal subsidence waves

The previous two subsections have explored the diurnal subsidence and vertical wind variability found in many of the near-coastal and remote tropical oceanic regions. However, examination of Figure 1 reveals several unique regions for which it is difficult to explain the diurnal variability with either classical land–sea breeze dynamics or gravity wave production from tropical oceanic deep convection. Two such regions are the area to the south and west of the Central American coast and the southeast Pacific west of Chile and Peru.

### *3.5.1. Central American coast*

Stretching from the Pacific waters adjacent to the Baja Peninsula to Nicaragua is a region with a particularly strong diurnal cycle (Figure 1(b) and (e)), which extends at least 10° from the coast. Close to the coast, peak divergence is found in the early afternoon, consistent with the sea-breeze circulation, if a little earlier than many other near-coastal regions (Figure 3). The coastline here is not concave, and there is strong mean convergence and upward vertical velocity as it is a region of strong deep convection during the summer months (Figure 1(a) and (d)). It is possible that in this region the deep convection helps to amplify the effect of the sea breeze with the gravity-wave mechanism of Mapes *et al*. (2003).

### *3.5.2. Southeast Pacific*

The southeast Pacific diurnal subsidence wave seen in Figure 1 is associated with the diurnal heating of the western slopes of the Andes Cordillera, which rise to a mean height of more than four kilometres over a distance of several thousand kilometres. This wave has been the focus of a numerical model study (Garreaud and Muñoz, 2004), which suggested that the wave is a propagating gravity wave extending up to approximately 5–6 km above the surface and propagating well over 1000 km from the coast. Our observations confirm that the wave structure is coherent even at 90°W, approximately 2000 km from the South American coast. Nowhere else on Earth does such a strong land-influenced signal propagate so far over the ocean. In this section we will explore the properties of this wave in some detail.

Figure 5 shows a Hovmüller plot along a line approximately perpendicular to the phase lines, i.e. along the direction of propagation of the subsidence wave. The time of maximum $D_0$ from the scatterometer coincides fairly well with the maximum downward vertical motion (strongest subsidence), demonstrating that the ECMWF model appears to capture the essence of the subsidence wave. The estimated wave propagation speed is approximately 25 m s$^{-1}$ and is consistent with the model-derived value of $\sim$30 m s$^{-1}$ reported in Garreaud and Muñoz (2004). The propagation speed $c$ is related to the depth of the heating, $H$, and the mean buoyancy frequency at levels below the heating, $N$, via $c = NH/\pi$ (Nicholls *et al*., 1991; Holton, 1992). A reasonable depth for the convective dry heating on the Western Andean slopes is $H = 6$ km (the Andes range in the region of interest itself rises to 4–5 km), and with $N \approx 0.012$ s$^{-1}$ throughout most of the tropical and subtropical low- to mid-troposphere, this leads to gravity-wave propagation speeds of $\sim$23 m s$^{-1}$, consistent with the observations.



DOI: 10.1002/qj

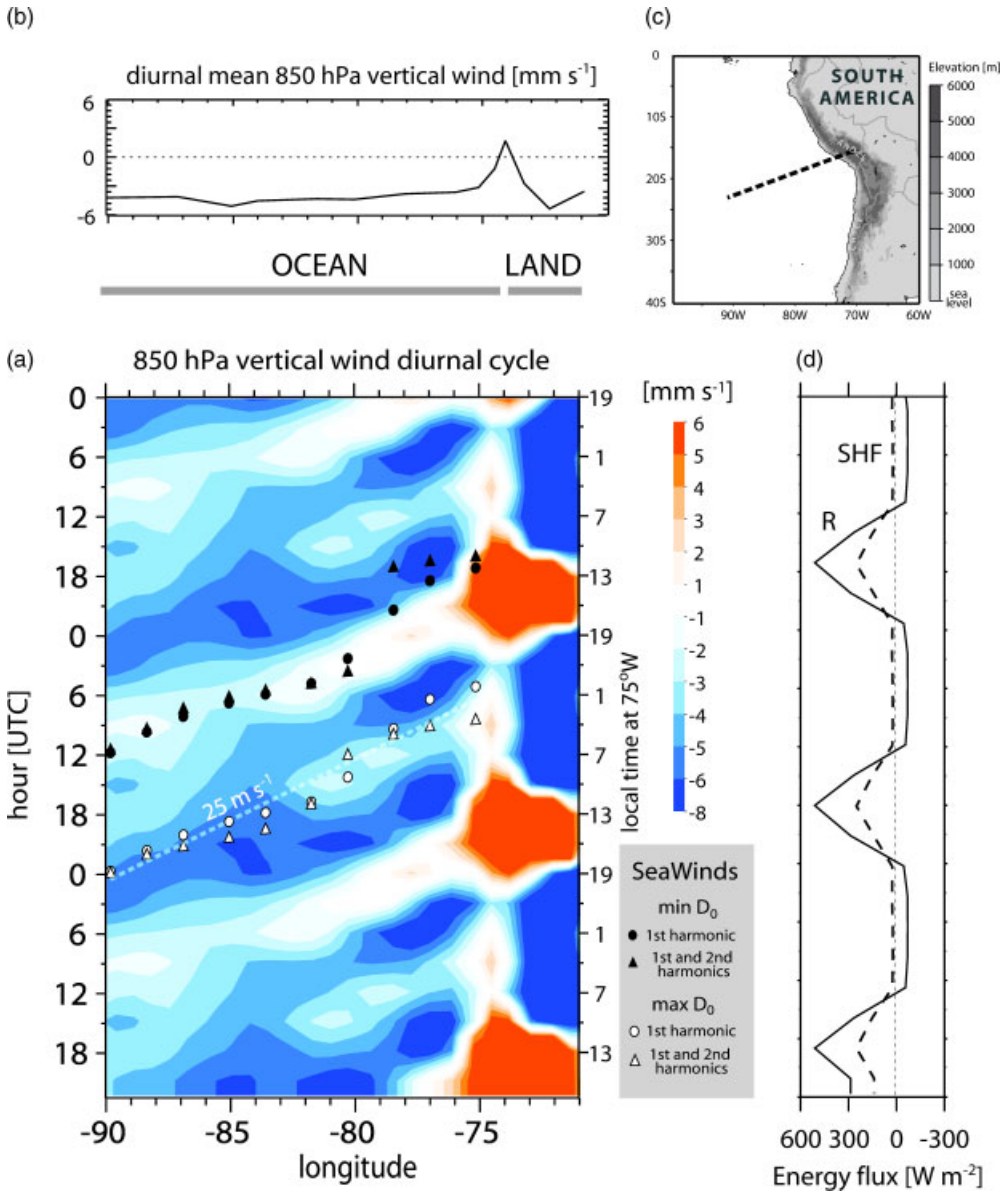


Figure 5. (a) Diurnal Hovmüller plot of $w_{850}$ (colours in the online figure) from ECMWF analyses along the line joining 23°S, 90°W and 15°S, 72°W; also shown are the times at which the scatterometer data indicate minimum (black) and maximum (white) surface divergence based on either first harmonic alone (circles) or on the first and second harmonics (triangles); the diurnal cycle is repeated three times for clarity. (b) Diurnal mean vertical wind at 850 hPa from ECWMF. (c) Geographic location with orography shown. (d) Mean sensible heat flux (SHF) and net radiative flux from the ECMWF analyses at a location (15°S, 72°W) on the western Andean slopes as a function of time. Local time at 75°W is UTC time minus 5 hours. This figure is available in colour online at www.interscience.wiley.com/journal/qj

The observed wave phase is also in excellent agreement with that simulated by Garreaud and Muñoz (2004) and from the idealized simulations of Nicholls *et al.* (1991), with the time of maximum subsidence and surface divergence at any given distance from the coast connected to the time of maximum heating by the wave-propagation speed. Thus, the maximum divergence at 75°W occurs about 3–4 h or so after the time of maximum heating on the Andes (the crest of which is located at 72°W along the cross-section line used to construct the Hovmüller plot), consistent with a propagation speed of ∼25 m $s^{-1}$ (∼1° $h^{-1}$). The scatterometer data and ECMWF data therefore provide support for a regionally extensive diurnal subsidence wave extending over a broad region of the southeast Pacific ocean.

The model simulations of Garreaud and Muñoz (2004) also suggest that the wave strengthens the diurnal cycle of cloudiness over the stratocumulus-capped marine boundary layer (MBL) to the west of South America. This may help to explain why the diurnal cycle of cloud liquid-water path in this region is the strongest of any of the regions of persistent subtropical low cloud (Wood *et al.*, 2002). The simulations also demonstrate that the wave amplitude is greatest during the Austral summer, and so the scatterometer data used here (April–September 2003) are providing observations of the wave during its weakest season.

In remote subtropical oceanic regions dominated by low clouds, the peak cloud liquid-water path (LWP) is observed to occur at 3–5 am local time (see Table 1 in



DOI: 10.1002/qj

Wood *et al*., 2002), consistent with daytime stabilization of the MBL by solar absorption in the cloud layer. This causes the MBL to decouple, thereby reducing the moisture supply to the cloud (Turton and Nicholls, 1987). To examine the diurnal cycle of LWP, we use data taken from a University of Wisconsin passive microwave climatology of cloud LWP (O'Dell *et al*., 2008), which uses a robust methodology to seamlessly combine LWP data from all available microwave imagers from 1988 to the present, starting from the retrieved LWP values from individual satellites using the retrieval algorithm of Hilburn and Wentz (2008). The climatology contains monthly mean values and corresponding diurnal cycles of LWP over the global oceans, as well as error estimates on all derived quantities based on the known statistical and systematic error sources.

To elucidate the propagating features in the LWP, we remove from the diurnal cycle of LWP (April–September) at each longitude the diurnal cycle of LWP at 20°S, 90°W. This location is sufficiently far from the shore that the diurnal cycle here represents primarily the effect of the solar absorption during the daytime. The amplitude (half of the maximum minus the minimum) of the diurnal cycle at 20°S, 90°W is close to 25 g $m^{-2}$, peaking at approximately 3 am local time. Figure 6 shows diurnal Hovmüller plots (time of day versus longitude) of these diurnal LWP anomalies, along the line shown in Figure 5. Clearly propagating features are apparent in the anomalies, with speeds roughly consistent with the speed of the diurnal subsidence waves observed in Seawinds data and the ECMWF data, suggesting a link between the propagating waves and the cloud LWP. The amplitude of the propagating component of the diurnal LWP cycle is comparable to that of the remote ocean diurnal cycle at 20°S, 90°W. At 75–80°W the anomalous LWP peaks during the late afternoon/early evening and thus results in a partial cancellation of the diurnal cycle due to solar absorption.

These results are consistent, at least qualitatively, with the interference of the diurnal subsidence with the diurnally modulated solar absorption. Enhanced subsidence impacts the cloud by lowering the cloud-top height, thus thinning the cloud. Conversely a minimum in subsidence (which at certain times of the day even becomes a net ascending motion in this region) results in a deepening of the boundary layer and a tendency towards thicker clouds. Landward of 80°W, upward motion during the afternoon appears to be sufficient to deepen the boundary layer significantly. The *rate of deepening* is maximal when the subsidence is minimal, and so the deepest boundary layer would occur some time after this (six hours for a truly sinusoidal diurnal wave). By late afternoon, therefore, this results in the enhanced diurnal anomaly in LWP seen in Figure 6. This LWP anomaly occurs at later times further from the land, consistent with the propagation of the diurnal subsidence wave. In addition, near the coast the enhanced subsidence during the early morning suppresses the early-morning LWP peak.

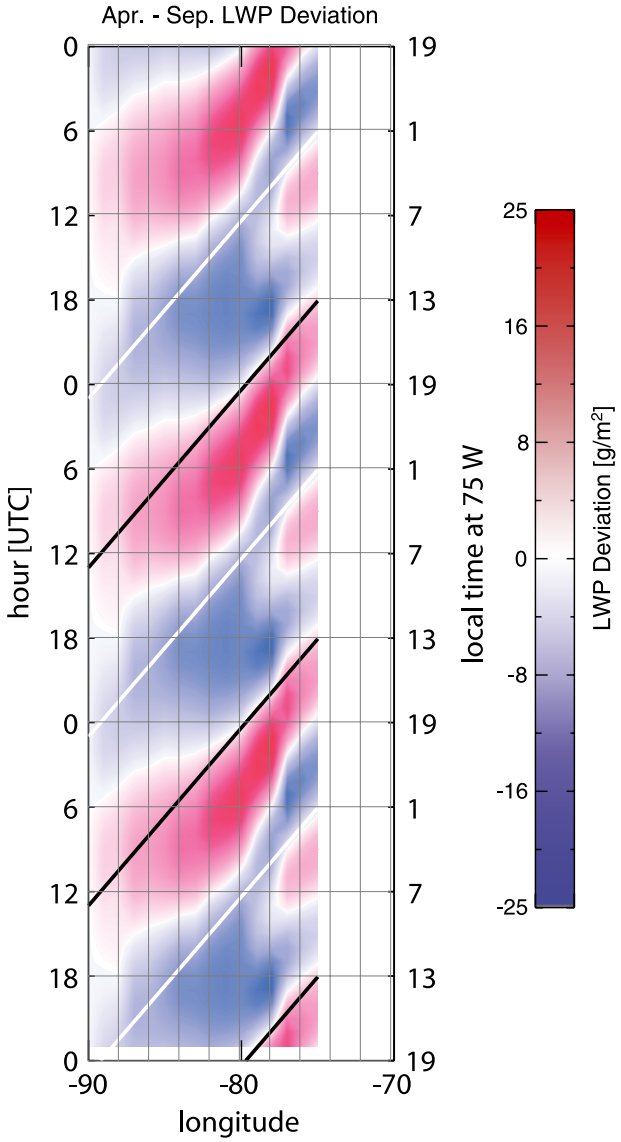


Figure 6. Hovmüller of LWP diurnal anomalies for April–July along the same line as in Figure 5 from the passive microwave climatology of O'Dell *et al*. (2008). To calculate the anomalies, the mean diurnal cycle at 20°S, 90°W (the far-field diurnal cycle) was removed from the diurnal cycle at each longitude. The white line reproduces the line of maximum subsidence shown in Figure 5 and the black line is the approximate time of the minimum subsidence. This figure is available in colour online at www.interscience.wiley.com/journal/qj

By the time the wave is further from shore, its effect is to enhance the diurnal cycle caused by solar absorption alone, because the minimum subsidence rate occurs around midnight (e.g. at 85°W) where it would help to deepen the MBL during the night and enhance the existing modulation of MBL depth and cloud. This is clearly seen in the positive LWP anomalies during the early-morning hours at 85°W in Figure 6. This is also supported by surface remote-sensing observations at 20°S, 85°W taken during the Eastern Pacific Investigation of Climate (EPIC) field programme (Bretherton *et al*., 2004; Caldwell *et al*., 2005), which show a very strong diurnal cycle of MBL depth in this region that is enhanced by constructive interference of the solar absorption and the diurnal subsidence.



DOI: 10.1002/qj

What does seem clear is that the diurnal subsidence wave has the ability to affect the diurnal cycle of cloud properties at large distances from the South American coast. More work will be required to examine its impact upon the diurnally averaged solar insolation at the ocean surface, and therefore the climate of the region.

## 4. Discussion and conclusions

The 4 × daily scatterometer data examined here reveal a rich pattern of diurnal variability extending over a large fraction of the world's oceans. It is natural to expect that the Coriolis force would limit the horizontal distance over which internal waves can propagate, which helps to explain why the remote oceanic diurnal features are largely confined to the region within 20–30° of the Equator (Figure 1). However, the six-month limits of the data record effectively rule out the detection of diurnal signals in regions of strong synoptic variability. Analyses of longer records (Dai and Deser, 1999) may be useful but lack the coverage that the scatterometer data can give.

The diurnally varying surface convergence is the signature of a diurnal cycle of vertical motion extending through a significant part of the lower troposphere. Subsidence in the lower troposphere relates to surface divergence by continuity. The significant agreement of the mean value and phase between ECMWF subsidence at 850 hPa and SeaWinds surface divergence (Figure 2) adds confidence in the accuracy of the mean and diurnal cycle of each of the two datasets. In the southeast Pacific region these motions appear to be sufficiently strong to significantly alter the diurnal cycle of cloud liquid-water content. Even if the mean LWP is unchanged by this diurnal dynamic variability, there may be rectification of the solar cycle with impacts on the upper ocean heat budget in coastal regions. Consider the southeast Pacific, where a strong diurnal subsidence wave is observed. Here, in the region out to 500–700 km from the coast, the diurnal wave partly offsets the daytime reduction in cloud liquid water expected from solar absorption alone. Thus the clouds may be more reflective during the daytime hours when the solar radiation is strongest than they would otherwise have been without the subsidence wave. This would result in a reduced solar flux at the surface which would cool the surface waters, thus enhancing the cooling due to oceanic upwelling. Observations of the diurnal cycle of cloud cover (rather than LWP) would be required to quantify this contribution of the Andes to upper-ocean cooling, but it is likely to be a significant effect that would additionally help to explain the extensive region of cold sea-surface temperature to the west of South America (Takahashi and Battisti, 2007). Whether and how the diurnal cycle of subsidence affects the cloud diurnal cycle elsewhere over the remote oceans remains to be explored.

In addition to the potential effects of the subsidence wave on the climatology of the southeast Pacific, we hypothesize that there may also be a connection between the waves and the transition from closed to open cellular convection, which occurs mainly at night (Wood *et al*., 2008). By enhancing the LWP, the enhanced thickening of the MBL caused by the subsidence wave during the late evening and early morning observed westward of 79°W would also add additional fuel to nocturnal precipitation formation, which is understood to be intimately connected with the formation of open cells (Stevens *et al*., 2005).

Finally, we have demonstrated that the diurnal cycle of surface convergence is a useful test for the ability of global models to represent physical processes accurately throughout the tropics. It would be a fruitful endeavour to combine the various extensive scatterometer datasets over the previous two decades to generate a dataset focused upon diurnal variability.

## Acknowledgements

We thank Rene Garreaud for valuable discussions on the nature of the diurnal cycle over the southeast Pacific Ocean. Nils Wedi at ECMWF developed the novel vertical velocity diagnostic analysis used in this work. This work was supported in part by NSF Grant 0433712. AMSR-E data are produced by Remote Sensing Systems and sponsored by the NASA Earth Science REASoN DISCOVER Project and the AMSR-E Science Team. Data are available at http://www.remss.com. QuikScat data are produced by Remote Sensing Systems and sponsored by the NASA Ocean Vector Winds Science Team.

## Appendix: Calculation of vertical velocity from ECMWF forecast fields

Calculation of vertical velocity $w$ from the default model output of omega ($\omega = \mathrm{d}p/\mathrm{d}t$) is complicated by the presence of pressure waves such as the semi-diurnal tidal wave prevalent in the tropics (Andrews *et al*., 1987; Janssen, 1999). This complication can be demonstrated by writing $w$ in the pressure coordinate system:

$$\begin{aligned} w &= \frac{\mathrm{d}z}{\mathrm{d}t} \\ &= \left.\frac{\partial z}{\partial t}\right|_p + v_p \cdot \nabla_p z + \omega \frac{\partial z}{\partial p} \\ &\approx \left.\frac{\partial z}{\partial t}\right|_p + v_p \cdot \nabla_p z - \frac{\omega}{\rho g}. \end{aligned} \tag{A1}$$

The last equation uses the hydrostatic equation. The second term is negligible for tidal waves because of their horizontal length-scales of ∼20 000 km. The difficulty of $\omega$ to $w$ conversion then lies in the determination of the pressure surface variations, i.e. the first term, such as tidal waves.

Therefore, the vertical velocity was specially diagnosed consistently with the semi-Lagrangian advection scheme used in the ECMWF model (see Temperton and Staniforth (1987) for a description of the numerical formulation).



DOI: 10.1002/qj

The vertical velocity at the trajectory mid-point $w^{1/2}$ between arrival and departure points $z^+$ and $z^0$ in this framework is written as

$$w^{1/2} = \frac{1}{2}(w^+ + w^0) = \frac{z^+ - z^0}{\Delta t}, \qquad \text{(A2)}$$

where $z^+$ is at a grid point and $z^0$ is found by interpolation of the geopotential to the departure point of the semi-Lagrangian trajectory. Equation (A2) is solved for the vertical velocity and the arrival point $w^+$.

## References


Andrews DG, Holton JR, Leovy CB. 1987. *Middle atmosphere dynamics*. Academic Press: San Diego.

Atkins NT, Wakimoto RM. 1997. Influence of the synoptic-scale flow on sea breezes observed during CaPE. *Mon. Weather Rev.* **125**: 2112–2130.

Atlas R, Hoffman RN, Leidner SM, Sienkiewicz J, Yu TW, Bloom SC, Brin E, Ardizzone J, Terry J, Bungato D, Jusem JC. 2001. The effects of marine winds from scatterometer data on weather analysis and forecasting. *Bull. Am. Meteorol. Soc.* **82**: 1965–1990.

Back LE, Bretherton CS. 2006. Geographic variability in the export of moist static energy and vertical motion profiles in the tropical Pacific. *Geophys. Res. Lett.* **33**: L17810. DOI:10.1029/2006GL026 672

Bretherton CS, Uttal T, Fairall CW, Yuter SE, Weller RA, Baumgardner D, Comstock K, Wood R. 2004. The EPIC 2001 stratocumulus study. *Bull. Am. Meteorol. Soc.* **85**: 967–977.

Caldwell P, Wood R, Bretherton CS. 2005. Mixed-layer budget analysis of the diurnal cycle of entrainment in SE Pacific stratocumulus. *J. Atmos. Sci.* **62**: 3775–3791.

Chelton DB, Freilich MH. 2005. Scatterometer-based assessment of 10m wind analyses from the operational ECMWF and NCEP numerical weather prediction models. *Mon. Weather Rev.* **133**: 409–429.

Chelton DB, Schlax MG, Freilich MH, Milliff RF. 2004. Satellite measurements reveal persistent small-scale features in ocean winds. *Science* **303**: 978–983.

Dai A, Deser C. 1999. Diurnal and semidiurnal variations in global surface wind and divergence fields. *J. Geophys. Res.* **104**: 31109–31125.

Deser C, Smith CA. 1998. Diurnal and semidiurnal variations of the surface wind field over the tropical pacific ocean. *J. Climate* **11**: 1730–1748.

Garreaud RD, Muñoz R. 2004. The diurnal cycle in circulation and cloudiness over the subtropical southeast Pacific: A modeling study. *J. Climate* **17**: 1699–1710.

Gille ST, Smith SGL, Lee SM. 2003. Measuring the sea breeze from Quikscat scatterometry. *Geophys. Res. Lett.* **30**: 1114.

Gille ST, Smith SGL, Statom NM. 2005. Global observations of the land breeze. *Geophys. Res. Lett.* **32**: L05605. DOI:10.1029/2004GL022 139

Hilburn KA, Wentz FJ. 2008. Mitigating the impact of RADCAL beacon contamination of F15 SSM/I ocean retrievals. *Geophys. Res. Lett.* **35**: L18806. DOI: 10.1029/2008GL034914

Holton JR. 1992. *An introduction to dynamic meteorology*. Academic Press: San Diego.

Isaksen L, Janssen PAEM. 2004. The benefit of ERS scatterometer winds in ECMWF's variational assimilation system. *Q. J. R. Meteorol. Soc.* **130**: 1793–1814.

Janssen PAEM. 1999. *On tides in the ECMWF model*. ECMWF Technical Memorandum 284. ECMWF: Reading, UK.

Kessler WS. 2002. Mean three-dimensional circulation in the northeast tropical Pacific. *J. Phys. Oceanogr.* **32**: 2457–2471.

Lungu T. 2002. *SeaWinds science data product user's manual, version 1.0*, Tech. Rep. JPL Doc D-21551. NASA Jet Propulsion Laboratory: Pasadena, CA. 128 pp.

Mapes BE, Warner TT, Xu M. 2003. Diurnal patterns of rainfall in northwestern South America. Part III: Diurnal gravity waves and nocturnal convection offshore. *Mon. Weather Rev.* **131**: 830–844.

Nesbitt SW, Zipser EJ. 2003. The diurnal cycle of rainfall and convective intensity according to three years of trmm measurements. *J. Climate* **16**: 1456–1475.

Nicholls ME, Pielke RA, Cotton WR. 1991. Thermally forced gravity waves in an atmosphere at rest. *J. Atmos. Sci.* **48**: 1869–1884.

O'Dell CW, Wentz FJ, Bennartz R. 2008. Cloud liquid water path from satellite-based passive microwave observations: a new climatology over the global oceans. *J. Climate.* **21**: 1721–1739.

Rotunno R. 1983. On the linear theory of the land and sea breeze. *J. Atmos. Sci.* **40**: 1999–2009.

Shige S, Takayabu WK, Tao WK, Shie CL. 2007. Spectral retrieval of latent heating profiles from TRMM PR data. Part II: Algorithm improvement and heating estimates over tropical ocean regions. *J. Appl. Meteorol. Climatol.* **46**: 1098–1124.

Small RJ, deSzoeke SP, Xie SP, O'Neill L, Seo H, Song Q, Cornillon P, Spall M, Minobe S. 2008. Air-sea interaction over ocean fronts and eddies. *Dyn. Atmos. Oceans* **45**: 274–319.

Stevens B, Vali G, Comstock K, Wood R, VanZanten M, Austin PH, Bretherton CS, Lenschow DH. 2005. Pockets of open cells (POCs) and drizzle in marine stratocumulus. *Bull. Am. Meteorol. Soc.* **86**: 51–57.

Takahashi K, Battisti DS. 2007. Processes controlling the mean tropical Pacific precipitation pattern. Part I: The Andes and the eastern Pacific ITCZ. *J. Climate* **14**: 3434–3451.

Temperton C, Staniforth A. 1987. An efficient two-time-level semi-Lagrangian semi-implicit integration scheme. *Q. J. R. Meteorol. Soc.* **57**: 2656–2670.

Turton JD, Nicholls S. 1987. A study of the diurnal variation of stratocumulus using a multiple mixed layer model. *Q. J. R. Meteorol. Soc.* **113**: 969–1009.

Wood R, Bretherton CS, Hartmann DL. 2002. Diurnal cycle of liquid water path over the subtropical and tropical oceans. *Geophys. Res. Lett.* **29**(23): 2092. DOI: 1029/2002GL015 371

Wood R, Comstock KK, Bretherton CS, Cornish C, Tomlinson J, Collins DR, Fairall C. 2008. Open cellular structure in marine stratocumulus sheets. *J. Geophys. Res.* **113**: D12207. DOI:10.1029/2007JD009596

Xie SP. 2004. Satellite observations of cool ocean-atmosphere interaction. *Bull. Am. Meteorol. Soc.* **85**: 195–208.

Yang S, Smith EA. 2006. Mechanisms for diurnal variability of global tropical rainfall observed from TRMM. *J. Climate* **19**: 5190–5226.

Zheng QA, Yan XH, Liu WT, Tang WQ, Kurz D. 1997. Seasonal and interannual variability of atmospheric convergence zones in the tropical Pacific observed with ERS-1 scatterometer. *Geophys. Res. Lett.* **24**: 261–263.